

Probing whole cell currents in high-frequency electrical fields: Identification of thermal effects

Michael Olapinski^a, Stephan Manus^a, Niels Fertig^b, Friedrich C. Simmel^{a,*}

^a Department of Physics and Center for Nanoscience, Ludwig-Maximilians-Universität München,
Geschwister-Scholl-Platz 1, 80539 Munich, Germany

^b Nanion Technologies, Erzgebirgstr. 4, 80335 Munich, Germany

Received 6 June 2007; received in revised form 18 August 2007; accepted 7 September 2007

Available online 16 September 2007

Abstract

An open-end coaxial probe is combined with a planar patch-clamp system to apply electric fields with GHz frequencies during conventional patch-clamp measurements. The combination of pulsed microwave irradiation and lock-in detection allows for the separation of fast and slow effects and hence facilitates the identification of thermal effects. The setup and the influence of radiation on the patch-clamp current are thoroughly characterized. For the independent optical verification of heating effects, a temperature microscopy technique is applied with high spatial, temporal and temperature resolution. It is shown that the effect of radiation at GHz frequencies on whole cell currents is predominantly thermal in nature in the case of RBL cells with an endogenous K_{ir} 2.1 channel.

© 2007 Elsevier B.V. All rights reserved.

Keywords: Biosensor; Patch-clamp; High-frequency techniques; Electrophysiology; Lab on a chip

1. Introduction

Patch-clamping is the most widely applied technique for the elucidation of ion channel function (Hamill et al., 1981; Hille, 2001; Sakmann and Neher, 1995). It allows for the precise measurement of the picoamp ionic currents flowing through transmembrane ion channels in live cells.

In recent years, a variety of chip-based, planar patch-clamp platforms have been developed (Fertig et al., 2002; Klemic et al., 2002; Kutchinsky et al., 2003; Pantoja et al., 2004). These platforms allow for the automatization of patch-clamp recordings and are therefore extremely well suited for automated screening applications. Moreover, as shown in the present work, a planar patch-clamp setup is also ideally suited for the combination of patch-clamp studies with other biophysical manipulation techniques. As such, the planar setup could serve as a general platform for bioelectronic hybrid sensors, in which the native biological sensing functions of ion channels and their gating behavior are exploited for technical applications (Cornell et al.,

1997; Terrettaz et al., 2001; Hirano et al., 2003; Tanaka and Sackmann, 2005). Recently, transient receptor potential (TRP) channels (Voets et al., 2005) and chemically engineered biological nanopores (Bayley and Cremer, 2001) have been suggested as particularly potent candidates for hybrid sensor applications.

Ionic currents through membrane channels may change in response to ligand binding, changes in membrane potential, mechanical stress or temperature. In the case of voltage-sensitive ion channels, it is assumed that “gating charges” sense the voltage drop over the membrane and lead to conformational rearrangements in the channel protein (Bezannila, 2000). In mechanosensitive and ligand-sensitive channels, similar processes result in channel opening. However, the structural transition from “open” to “closed channel” does not occur in a single step—a large number of internal rearrangements precede the final opening step (Magleby, 2003). Traditional patch-clamp recordings mainly yield information over the final opening transition. To gain more information about the cellular response to external stimuli in terms of ion channel currents, a combination of patch-clamp recording with other techniques is required.

Several research groups have utilized fluorescence resonance energy transfer to study the conformational changes of ion channel receptors (Blunck et al., 2004; Posson et al., 2005; Riven et

* Corresponding author.

E-mail address: simmel@lmu.de (F.C. Simmel).

al., 2006). In addition, this issue was addressed by genetic engineering of ion channel proteins (Starace and Bezanilla, 2004), and also in molecular dynamics simulations.

In this work, we investigate another approach to study internal rearrangements of ion channels, namely the utilization of high-frequency electronic techniques. Physiological systems contain various constituents with dipolar moments that are susceptible to electrical fields. Besides the well-known “thermal” effect of uniform solution heating (the relaxation frequency of water at 25 °C is around 20 GHz), two other mechanisms are relevant. First, energy absorption on the molecular level due to relaxation or resonance effects (“microthermal heating”), and second, the induction of an electric field across the cell membrane, resulting in a possible gating of the ion channels embedded.

The large dipolar moments of proteins (Gurd and Rothgeb, 1979; Pethig, 1984) provide a target for external electrical fields. Rotational relaxation frequencies in aqueous environment are found to be in the kHz–MHz range (Grant et al., 1978; Pethig, 1984). Smaller protein subunits or biomolecules exhibit much higher relaxation frequencies, e.g. lipid headgroups (around 100 MHz) (Kaatze, 1990), amino acids (up to the GHz range) (Foster and Schwan, 1989) and interfacial water with reduced relaxation frequencies in the GHz range (Kaatze, 1990; Steinhoff et al., 1993). Other fast biochemical processes comprise protein unfolding (below 10 ns) (Steel et al., 2006), ligand translocation in myoglobin (several 100 ps) (Schotte et al., 2003), protein hydrogen bond (Kolano et al., 2006) and vibrational dynamics of transmembrane helices (ps–ns) (Mukherjee et al., 2006). Non-thermal effects of GHz irradiation have been shown for EGFP fluorescence (Coptly et al., 2006), and for folding of lactoglobulin (Bohr and Bohr, 2000).

In the context of voltage-gated ion channels, gating is associated with the movement of a gating charge (Bezanilla, 2000). Admittance studies on gating charge movement (Horrigan and Aldrich, 1999) have revealed relaxation times of order 100 μ s. Charge motion within membranes depends on the transmembrane potential drop. At low frequencies, an externally applied voltage almost entirely drops across the membrane, resulting in local field strengths 1000 times higher than the applied voltage divided by the electrode distance. The field strength is considerably reduced at higher frequencies. Numerical calculations yield a reduction of the local field by a factor of 200 for low GHz frequencies and different cell and membrane geometries (Apollonio et al., 2000; Eibert et al., 1999; Sebastián et al., 2001). AC fields up to 40 MHz have been shown to induce a rectified current in plant cells (Pickard and Barsoum, 1981), and AC electroporation studies show that induced transmembrane voltages are at least effective up to 500 MHz (Chang, 1989).

To date, there are only few investigations of ion channel currents under exposure to high-frequency electrical fields. Recently, a single channel patch-clamp study on rat sensory neurons exposed to electric fields oscillating at 50 Hz and 900 MHz was presented (Marchionni et al., 2006), based on a large coplanar waveguide setup. Earlier studies involved artificial lipid bilayers containing channel-forming peptides (Aleksiev and Ziskin, 1995; Sandblom and Theander, 1991) and whole-cell currents in neurons (Aleksiev et al., 2000) exposed to fixed

GHz frequencies through rectangular waveguides, or large plant cells in a microstrip line below 50 MHz (Pickard and Barsoum, 1981). To our knowledge, no electrophysiological studies with frequencies over a wide range in the GHz regime are available.

Due to the diversity of possible effects of high-frequency irradiation on physiological systems, it is of great importance to be able to distinguish between the thermal and dynamical effects of electromagnetic radiation. In the following, we introduce a novel experimental setup for the determination of ion channel currents under the influence of high-frequency (HF) electric fields (Fig. 1). To this end, a HF signal is pulsed at a lower frequency and the current response is detected using lock-in techniques. Variation of the pulse frequency allows for the separation of fast and slow processes, i.e. non-thermal from thermal effects. The use of lock-in demodulation filters out the influence of current variations and drift.

2. Materials and methods

2.1. Experimental setup

The application of high-frequency electrical fields, e.g. in dielectric spectroscopy, is typically achieved by placing the sample within a closed transmission line (Pottel et al., 1984) or at the tip of an open-end coaxial probe (Stuchly and Stuchly, 1980). Open geometries like coplanar waveguides have also been used for sensor applications (Chen et al., 2007; Facer et al., 2001; Olapinski et al., 2006). To combine wide frequency tunability and simple handling in the context of a chip-based patch-clamp system, in the present study an open-end coaxial probe was chosen (Fig. 1). The HF probe is combined with Nanion’s Port-a-Patch system connected to a patch-clamp amplifier. HF power is

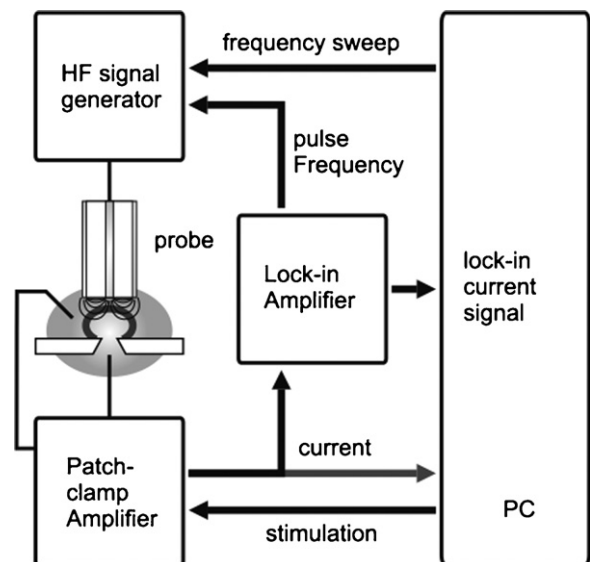


Fig. 1. Experimental setup. Patch-clamp recordings are performed with a chip-based system as described in (Bruggemann et al., 2006; Fertig et al., 2002). An open-end coaxial probe for the application of pulsed HF radiation is placed in the vicinity of the cell using a micromanipulator. The membrane current measured by a patch-clamp amplifier is fed into a lock-in amplifier and demodulated with the HF pulse frequency.

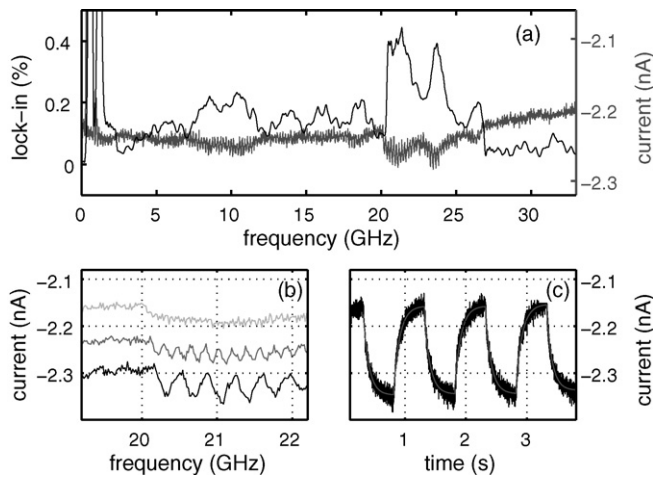


Fig. 2. (a) Simultaneous recording of current (gray, right scale) and lock-in signal (black, left scale). Current flow was measured through the open chip aperture. HF was pulsed with 2 Hz and swept from 2 GHz to 33 GHz. The application of pulsed RF results in strongly frequency dependent conductivity changes. (b) Magnified current traces for different pulse frequencies (black, 1 Hz, dark gray, 2 Hz, light gray, 5 Hz). The HF pulses can be directly observed in the current trace. (c) Current vs. time trace with improved alignment of probe and chip aperture (black). HF at 22 GHz (cw) was pulsed with 1 Hz. Exponential fits to the data are displayed in gray.

supplied by a signal generator with pulse modulation. The patch-clamp current recorded through the chip is fed into a lock-in amplifier and demodulated with the pulse frequency. A function generator produces the TTL signal for pulse modulation and as a reference for the lock-in amplifier. Details on the equipment, electronic setup, cell culture and electrophysiology can be found in [Supplementary data](#).

2.2. HF exposure experiments

The HF electrical field is applied through an open-end coaxial probe, mounted on a micromanipulator stage. Before an exposure experiment its position with respect to the cell and chip aperture is optimized, which is assessed by the magnitude of the thermal effect of HF irradiation (22 GHz pulsed at 1 Hz) on the conductivity (Fig. 2c).

In an exposure experiment, the cell is clamped to a specific potential for 230 s. After 5 s, the current offset is subtracted and fed into the lock-in amplifier, 5 s later a HF sweep is triggered and the pulsed exposure is started for 200 s. After the sweep, the lock-in signal is recorded for another 5 s without HF exposure. Finally, a voltage ramp is applied to verify the cell and ion channel vitality.

2.3. Fluorescence microscopy and spectrometry

Fluorescence microscopy was performed on an Olympus IX71 with a cooled CCD camera (Photometrics Coolsnap HQ), computer controlled shutter and acquisition software (MetaVue, Universal Imaging Corporation). For fluorescence temperature imaging, solutions of 100 μ M fluorescein in 20 mM ethylene diamine (pH 6.54) were prepared. The temperature dependence of a mixture with 200 nM fluorescein was measured in a

temperature-controlled fluorescence spectrometer (Jobin Yvon Fluorolog-3, shown in [Supplementary data](#)).

3. Results and discussion

3.1. Thermal effect of HF pulses

The experimental setup was first characterized thoroughly in the absence of cells. For this purpose, currents through the bare chip aperture were measured as a function of the applied frequency. In Fig. 2a, a current trace (gray, right scale) is shown which was recorded during a frequency sweep from 10 MHz to 33 GHz. A strong variation of the measured DC current as a function of irradiation frequency is observed. The response of the chip system to HF irradiation was also characterized using the lock-in technique described in Section 2.1 and in [Supplementary data](#). It can be seen from Fig. 2a (black, left scale) that the measured lock-in signal well reproduces the main features of the current signal. As discussed in Section 1, one of the major effects of HF irradiation in the GHz range is heating of the buffer solution. We here show that (1) the observed current response in the cell-free configuration is consistent with such a thermal effect, and (2) that heating is suppressed at higher pulse frequencies.

In our chip-probe system, the temperature increase takes place predominantly in the thin disk of solution ($V \approx 0.5 \mu$) between the glass chip and the probe. A thorough computational treatment of the dissipation problem is complicated by the complex geometry and the various materials involved. If we assume that the disk has homogeneous but time dependent temperature $T(t)$ and the environment is a heat reservoir of constant temperature T_R , dissipation can be treated by Newton's law of cooling,

$$\frac{dT}{dt} = -\frac{1}{\tau}(T - T_R) + \frac{P_{\text{abs}}}{\tilde{c}}, \quad (1)$$

where τ is the characteristic time for decay of the temperature difference (reflecting geometry and materials), P_{abs} is the absorbed heating power and \tilde{c} is the heat capacity of the volume. The solution to this equation yields exponential temperature changes according to

$$T(t) = (T(0) - T_R - \Delta T_H) \exp\left(-\frac{t}{\tau}\right) + T_R + \Delta T_H \quad \text{with} \quad (2)$$

$$\Delta T_H = P_{\text{abs}} \frac{\tau}{\tilde{c}}$$

Here, ΔT_H is the temperature increase after an infinite time of heating with P_{abs} . For many consecutive cycles of heating and cooling of equal duration, an average temperature $T_R + \Delta T_H/2$ is approached. The amplitude of temperature variation $\Delta T(t_c)$ within each cycle depends on the cycle duration t_c and is given by

$$\Delta T(t_c) = \Delta T_H \frac{1 - \exp(-t_c/\tau)}{1 + \exp(-t_c/\tau)} \quad (3)$$

Temperature variations translate into changes in ionic conductance via the temperature dependence of the viscosity η of the solution. According to Walden's rule, the ionic mobilities and

therefore the conductance G is inversely proportional to η . For the small temperature variations in our experiment, the temperature dependence of $1/\eta$ can be linearized, and hence $\Delta G \sim \Delta T$. At an applied constant DC voltage, periodic temperature variations are directly reflected in periodic current variations ΔI and can therefore be detected by our lock-in scheme. As already proposed by Pickard and Rosenbaum, 1978, the dependence of ΔT on t_c offers a means to discriminate between processes of different temporal behavior: for pulse frequencies well above $1/\tau$, the effect of solution heating disappears in the lock-in signal. By contrast, faster resonant processes as well as microthermal heating effects should still be detected.

The current traces shown in Fig. 2b and c are consistent with a heating effect: when the chip is irradiated with pulsed HF, the amplitude of the current variation decreases for higher modulation frequencies (Fig. 2b) and the current traces corresponding to heating and cooling cycles can be fit with an exponential $I(t) = I_0 + \Delta I(1 - \exp(-t/\tau))$ (Fig. 2c). The average value for τ is 96 ms and 103 ms for heating and cooling, respectively.

A detailed study of the influence of HF power, DC current and HF modulation frequency on the lock-in signal can be found in Supplementary data and supports the thermal origin of the signals above 2 GHz. However, the large signal at lower frequencies (Fig. 2a) displays HF power dependence, but no dependence on current or pulse frequency. Extensive control experiments revealed that in the low GHz range the HF signal is directly picked up by the patch-clamp preamplifier headstage. This proves that the field penetrates solution and chip aperture and, in principle, should be capable of influencing a cell (cf. Fig. 1).

The thermal signals (Fig. 2a) show a pronounced ‘dome’-like structure between 20 GHz and 26.5 GHz. This feature can be traced back to a combination of different effects. First and foremost, the dielectric absorption of water has a T -dependent maximum around 20 GHz. Furthermore, the available maximum power from the signal generator varies for different frequency ranges. In fact, the dome structure closely resembles the frequency response of the 20–26.5 GHz band where maximum power is available (Hewlett Packard, User’s Guide). Finally, power variations can result from different coupling efficiencies and power reflection from the probe end.

We independently verified the thermal effect of HF irradiation using fluorescence techniques. For that purpose a “temperature microscopy” method was developed similar to that by Duhr et al. (Duhr et al., 2004). A solution of the pH dependent dye fluorescein was prepared in the temperature-dependent pH buffer ethylene diamine such that a temperature change is translated into a change in the fluorescence intensity. From fluorescence spectrometry (Supplementary data), an almost linear fluorescence decrease of $1.82\%/^{\circ}\text{C}$ is obtained. In order to visualize the heating effect directly, the HF setup was placed onto an inverted fluorescence microscope, with the patch-clamp chip replaced by a cover slip (brightfield image in Fig. 3a). The fluorescein-buffer mixture was then applied between probe and glass slide and a series of fluorescence images was taken, while the HF power (22 GHz, 25 dBm) was alternately switched on and off.

For each image the fluorescence intensity was averaged over 20×20 pixels and the normalized difference of two images just before the start and end of the irradiation was calculated. The difference image reflects the temperature increase during the

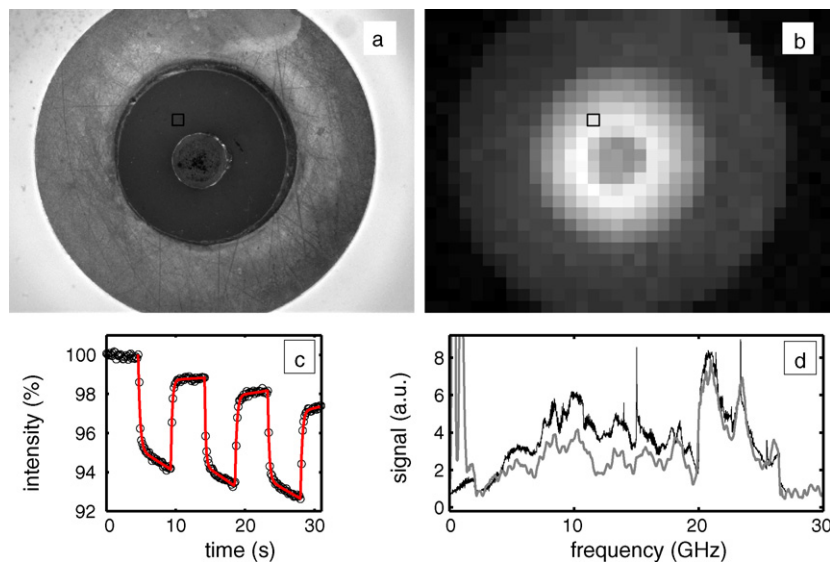


Fig. 3. (a) Brightfield microscopy image of the HF probe tip. For fluorescence microscopy, fluorescein solution was confined between probe tip and a glass cover slide. Fluorescence images are taken while HF power (22 GHz, 25 dBm) is switched on and off. (b) Normalized difference of fluorescence intensity, averaged over 20×20 pixels, taken before and after HF exposure, corresponding to a temperature profile of the solution between probe and cover glass (grayscale from 0% to 6.5%, equivalent to 3.6°C). (c) Time trace of the intensity averaged over the highlighted square in (b). The onset and end of HF irradiation cycles can be clearly observed (cf. current signal in Fig. 2c). The data is fit with an exponential plus a linear term (gray). (d) Comparison of the fluorescence intensity change during a HF frequency sweep (black, linear baseline subtracted) with a lock-in trace of the current variation through the chip aperture (gray). Both traces agree very well except for the features below 2 GHz, which have no thermal origin. Short spikes in the fluorescence trace originate from dust particles crossing the field of view during the measurement.

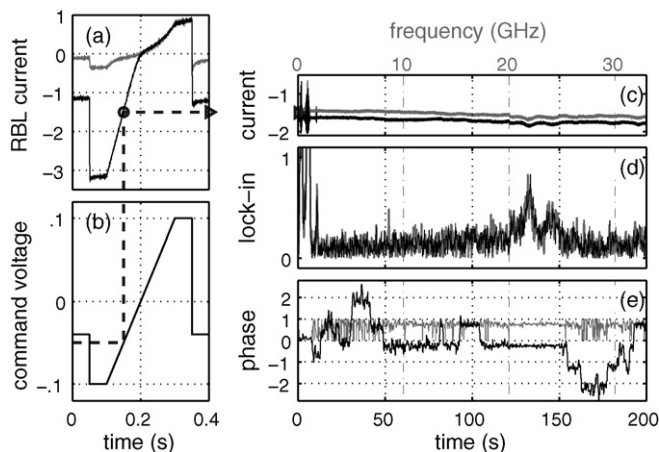


Fig. 4. Illustration of a typical whole cell experiment. (a and b) Command cell potential (V) and whole cell current (nA) of an RBL cell with high (black) and low (gray) external potassium concentration. Inward rectification of $K_{ir} 2.1$ channels is observed in the black graph. The dashed line and the circle indicate the parameters for the HF exposure experiment in (c). (c) Whole cell currents during HF exposure, two consecutive traces (gray and black). The HF is swept from 10 MHz to 33 GHz in 200 s and pulsed with 170 Hz. Lock-in integration time is 100 ms. (d) Rescaled lock-in amplitude signal $\Delta I/I$ in units of 10^{-3} . The electronic pickup below 2 GHz and the ‘dome’ structure between 20 GHz and 26.5 GHz is visible in the lock-in as well as the current signal (c). (e) Lock-in phase (in full cycles) for the black trace in (c), as sampled from the amplifier (gray) and with phase jumps larger than π ‘unwrapped’ to the adjacent phase interval (black). Phase stability provides a measure of the reliability of the lock-in amplitude data, while phase jumps and large noise amplitudes indicate periods of unlock, e.g. between 20 GHz and 26.5 GHz, where the lock-in signal is largest, the phase is most stable.

irradiation with lateral resolution (Fig. 3b). We find a maximum temperature increase of 3.6°C . A time trace of the fluorescence (Fig. 3c) is well fit by $I(t) = I_0 + \Delta I(1 - \exp(-t/\tau)) + \delta I \times t$, with a linear term accounting for global heating of the reservoir by long HF exposure and microscope illumination. The average values for τ in Fig. 3c are 0.22 s and 0.25 s for heating and cooling, respectively. The temporal resolution of “temperature microscopy” is currently limited by the CCD integration time of roughly 100 ms with a lateral resolution of about $100\ \mu\text{m}$ ($4\times$ objective), while the ΔT -resolution is 0.1°C . This could be improved considerably with higher power objectives and more sensitive detection equipment. Our method even allows spatially resolved temperature measurements during a frequency sweep (Fig. 3d). The comparison of the optical with the electronic data in Fig. 3d displays very good agreement above 2 GHz, which confirms the thermal origin of the lock-in signal. As expected, the features below 2 GHz are non-thermal and are not reproduced in the fluorescence data.

3.2. Patch-clamp of live cells under application of HF pulses

Electrophysiological measurements of live rat basophil leukemia (RBL) cells with an endogenous inward rectifying potassium channel $K_{ir} 2.1$ were conducted with the planar patch-clamp chip as summarized in Section 2 and in Supplementary data. After whole-cell conditions were obtained, voltage ramps

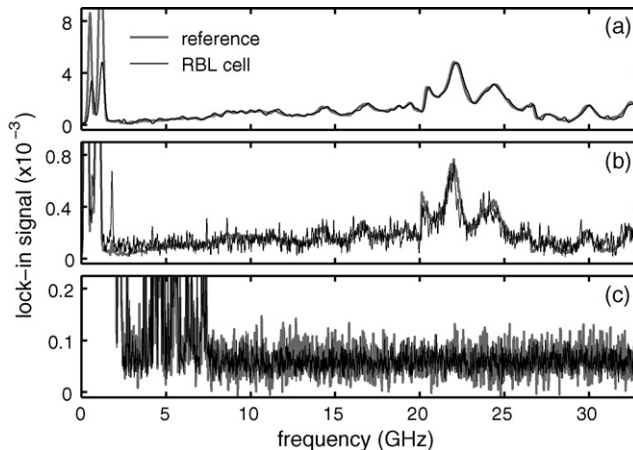


Fig. 5. Averaged lock-in signals of RBL whole cell currents under HF exposure from 10 MHz to 33 GHz compared to reference traces obtained from the open chip aperture. (a) Pulse frequency 20 Hz, lock-in integration time 500 ms. The thermal signal is clearly visible and the RBL signal closely follows that signal. No non-thermal signature can be discerned. Averaging is $2\times/2\times$ for RBL/reference, respectively. (b) Pulse frequency 170 Hz, lock-in integration time 100 ms, averaging $2\times/4\times$. The signal amplitude of the thermal features is much smaller as compared to (a). Yet, possible non-thermal HF signatures like spikes or intervals deviating from the reference trace are not visible. (c) Pulse frequency 5520 Hz, 50 ms integration time, averaging $4\times/12\times$. Thermal signatures are suppressed. However, additional artifacts appear below 8 GHz, which become visible due to the reduced thermal signal and the smaller integration time.

(Fig. 4b) were applied to verify the vitality of the cell and the $K_{ir} 2.1$ channels (Fig. 4a). For the HF exposure experiment, the holding potential was chosen to obtain a current of about 1.5 nA. Before the start of each experiment, the probe was aligned with cell and aperture as described in the Section 2. In Fig. 4c, two consecutive current traces are shown during exposure of the cell with HF between 10 MHz and 33 GHz. Fig. 4d and e display the corresponding lock-in amplitude and phase traces for 170 Hz modulation frequency and 100 ms lock-in integration time, respectively. In the current and lock-in traces the ‘dome’ structure and the non-thermal signal below 2 GHz can be recognized. Ranges for which the phase is stable indicate a good lock to the modulation frequency. In order to make lock-in traces of several different measurements and cells comparable, a relative current variation $\Delta I/I$ is obtained by rescaling the data by multiplication with

$$\frac{(\text{lock-in full scale sensitivity})}{(\text{lock-in full scale output voltage}) \times (\text{patch-clamp amplifier gain})}$$

and division by the running average of the current signal over the lock-in integration time. The traces in Fig. 4c and d show very good agreement and reproducibility between two measurements. Although the current in the second trace is increased, probably due to evaporation of liquid and increased salt concentration or a slightly increased leakage current, the rescaled lock-in traces match very well. In many experiments, even between different cells, the signatures were very well reproduced albeit scaled differently, as is expected for thermal effects with the HF probe positioned differently. This finding allows for the averaging of several traces to further reduce the noise background.

In Fig. 5, averaged lock-in traces of RBL signals for 20 Hz, 170 Hz and 5520 Hz modulation frequency and HF frequency sweeps from 10 MHz to 33 GHz are displayed and compared with reference traces obtained from the bare chip aperture. Deviations of the RBL signals from the reference traces would indicate a cell-specific HF effect additional to the common heating effect. In Fig. 5a, however, no deviations from the thermal reference traces are observed. For pulse modulations of 20 Hz the thermal signal is strong and dominates the spectra, masking possible non-thermal or microthermal HF effects. For 170 Hz pulse modulation, (Fig. 5b) the signal is already reduced considerably. The thermal feature is still clearly visible. In Fig. 5c (5520 Hz pulse modulation), the thermal signatures are largely suppressed and only a very low signal (below $\Delta I/I = 10^{-4}$) is measured. More intense averaging could further improve this sensitivity.

The good agreement of RBL and reference data within 0.5×10^{-4} relative current variation indicate that no non-thermal effects of this magnitude are present. However, for the 5520 Hz modulation several additional features become visible in the range up to 8 GHz, effectively masking this frequency range. Further improvements of the setup are required here to make this important frequency range accessible to more sensitive detection. One approach would be to introduce a HF shielding between the chip inside and the cytosolic patch-clamp electrode, allowing the HF to influence the cell but not the amplifier circuit. Additionally, modification of the probe geometry could avoid direct irradiation into the headstage.

In the measurements presented, the functionality of the setup could be demonstrated on live cells, establishing that the effects are predominantly thermal in nature. However, the ion channels were investigated in the linear regime of their current–voltage relation (Fig. 4a). It will be highly interesting to extend the study to the nonlinear regime, implying different holding potentials and lower absolute current levels. We are currently using the setup presented to study voltage-sensitive ion channels with a more complex gating behavior.

4. Conclusion

We have presented a novel setup for the application of HF electrical fields to cells or bilayer membranes during patch-clamp experiments. A planar chip-based patch-clamp system was used and proved particularly suited for the integration with additional components like a coaxial HF probe. The suitability of the open-end probe for the application of HF fields was demonstrated and quantified, and the thermal effect of the irradiation was identified. A temperature microscopy technique with a temperature sensitivity of 0.1°C and high temporal and lateral resolution was developed and applied to quantify field distribution and thermal effects.

Using a lock-in technique and pulsed HF irradiation, it was shown that the thermal effect of HF exposure can be suppressed and the signal is largely insensitive to current variations and drift. This offers the possibility of detecting HF induced variations in whole cell current as small as 0.5×10^{-4} . The technique was demonstrated in patch-clamp measurements on endogenous K_{ir}

2.1 channels in RBL cells. Our data indicate that for this channel type the influence of HF irradiation on ion channel currents is predominantly thermal in nature. Further improvements of the setup are required to achieve even higher sensitivity and extend the frequency range studied to lower frequencies. Future investigations will be extended to other voltage-gated ion channels with potential HF sensitivity. Furthermore, the thermal effects induced by the HF irradiation may be directly utilized for the study of strongly temperature sensitive ion channels such as those of the TRP family (Voets et al., 2005). More generally, we have shown that a planar patch-clamp setup is an ideal platform for the study of ion channel currents of live cells exposed to external stimuli, which may be utilized for the development of novel cell-based bioelectronic sensors.

Acknowledgements

The authors thank J.P. Kotthaus, J. Behrends, G. Schwake, S. Kempter and J.O. Rädler for help and useful discussions. Financial support by the BMBF (BMBF 13N8363, 13N8364) and the DFG (SI 761/2-1/2/3) is gratefully acknowledged. M.O. is supported by the IDK-NBT Munich.

Appendix A. Supplementary data

Supplementary data associated with this article can be found, in the online version, at doi:10.1016/j.bios.2007.09.004.

References

- Alekseev, S.I., Ziskin, M.C., 1995. *Bioelectromagnetics* 16 (2), 124.
- Alekseev, S.I., Ziskin, M.S., Kochetkova, N.V., 2000. *Crit. Rev. Biomed. Eng.* 28 (5–6), 52–59.
- Apollonio, F., Liberti, M., d’Inzeo, G., Tarricone, L., 2000. *IEEE Trans. Microwave Theory* 48 (11), 2082.
- Bayley, H., Cremer, P.S., 2001. *Nature* 413 (6852), 226–230.
- Bezanilla, F., 2000. *Physiol. Rev.* 80 (2), 555–592.
- Blunck, R., Starace, D.M., Correa, A.M., Bezanilla, F., 2004. *Biophys. J.* 86 (6), 3966.
- Bohr, H., Bohr, J., 2000. *Phys. Rev. E* 61 (4), 4310–4314.
- Bruggemann, A., Stoelzle, S., George, M., Behrends, J.C., Fertig, N., 2006. *Small* 2 (7), 840–846.
- Chang, D.C., 1989. *Biophys. J.* 56 (4), 641–652.
- Chen, Q., Roitman, D., Knoesen, A., 2007. *Sens. Actuators A: Phys.* 133 (2), 480–485.
- Coty, A.B., Neve-Oz, Y., Barak, I., Golosovsky, M., Davidov, D., 2006. *Biophys. J.* 91 (4), 1413–1423.
- Cornell, B.A., Braach-Maksyitis, V.L.B., King, L.G., Osman, P.D.J., Raguse, B., Wiczorek, L., Pace, R.J., 1997. *Nature* 387 (6633), 580–583.
- Duhr, S., Arduini, S., Braun, D., 2004. *Eur. J. Phys. E* 15 (3), 277–286.
- Eibert, T.F., Alaydrus, M., Wilczewski, F., Hansen, V.W., 1999. *IEEE Trans. Biomed. Eng.* 46 (8), 1013–1021.
- Facer, G.R., Notterman, D.A., Sohn, L.L., 2001. *Appl. Phys. Lett.* 78 (7), 996–998.
- Fertig, N., Blick, R.H., Behrends, J.C., 2002. *Biophys. J.* 82 (6), 3056–3062.
- Foster, K.R., Schwan, H.P., 1989. *Crit. Rev. Biomed. Eng.* 17 (1), 25–104.
- Grant, E.H., Sheppard, R.J., South, G.P., 1978. *Dielectric Behaviour of Biological Molecules in Solution*. Oxford University Press, Oxford.
- Gurd, F.R.N., Rothgeb, T.M., 1979. *Adv. Protein Chem.* 33, 73–165.
- Hamill, O.P., Marty, A., Neher, E., Sakmann, B., Sigworth, F.J., 1981. *Pflügers Archiv. Eur. J. Physiol.* 391 (2), 85–100.

- Hille, B., 2001. *Ion Channels of Excitable Membranes*, third ed. Sinauer Associates, Sunderland.
- Hirano, A., Wakabayashi, M., Matsuno, Y., Sugawara, M., 2003. *Biosens. Bioelectron.* 18 (8), 973–983.
- Horrigan, F.T., Aldrich, R.W., 1999. *J. Gen. Physiol.* 114 (2), 305.
- Kaatze, U., 1990. *Phys. Med. Biol.* 35 (12), 1663–1681.
- Klemic, K.G., Klemic, J.F., Reed, M.A., Sigworth, F.J., 2002. *Biosens. Bioelectron.* 17 (6–7), 597.
- Kolano, C., Helbing, J., Kozinski, M., Sander, W., Hamm, P., 2006. *Nature* 444 (7118), 469.
- Kutchinsky, J., Friis, S., Asmild, M., Taboryski, R., Pedersen, S., Vestergaard, R.K., Jacobsen, R.B., Krzywkowski, K., Schroder, R.L., Ljungstrom, T., Helix, N., Sorensen, C.B., Bech, M., Willumsen, N.J., 2003. *Assay Drug Dev. Technol.* 1 (5), 685.
- Magleby, R.L., 2003. *J. Gen. Physiol.* 121 (2), 81.
- Marchionni, I., Paffi, A., Pellegrino, M., Liberti, M., Apollonio, F., Abeti, R., Fontana, F., D'Inzeo, G., Mazzanti, M., 2006. *Biochim. Biophys. Acta: Biomembr.* 1758 (5), 597.
- Mukherjee, P., Kass, I., Arkin, I., Zanni, M.T., 2006. *Proc. Natl. Acad. Sci. U.S.A.* 103 (22), 8571.
- Olapinski, M., Manus, S., George, M., Bruggemann, A., Fertig, N., Simmel, F.C., 2006. *Appl. Phys. Lett.* 88 (1), 013902.
- Pantoja, R., Nagaraj, J.M., Starace, D.M., Melosh, N.A., Blunck, R., Bezanilla, F., Heath, J.R., 2004. *Biosens. Bioelectron.* 20 (3), 509.
- Pethig, R., 1984. *IEEE Trans. Electr. Insul.* 19 (5), 453–474.
- Pickard, W.F., Barsoum, Y.H., 1981. *J. Membr. Biol.* 61 (1), 39–54.
- Pickard, W.F., Rosenbaum, F.J., 1978. *Math. Biosci.* 39 (3–4), 235–253.
- Posson, D.J., Ge, P.H., Miller, C., Bezanilla, F., Selvin, P.R., 2005. *Nature* 436 (7052), 848–851.
- Pottel, R., Gopel, K.D., Henze, R., Kaatz, U., Uhlendorf, V., 1984. *Biophys. Chem.* 19 (3), 233–244.
- Riven, I., Iwanir, S., Reuveny, E., 2006. *Neuron* 51 (5), 561.
- Sakmann, B., Neher, E., 1995. *Single Channel Recording*. Plenum Press, New York.
- Sandblom, J., Theander, S., 1991. *Bioelectromagnetics* 12 (1), 9–20.
- Schotte, F., Lim, M.H., Jackson, T.A., Smirnov, A.V., Soman, J., Olson, J.S., Phillips, G.N., Wulff, M., Anfinrud, P.A., 2003. *Science* 300 (5627), 1944.
- Sebastián, J.L., Munoz, S., Sancho, M., Miranda, J.M., 2001. *Phys. Med. Biol.* 46 (1), 213.
- Starace, D.M., Bezanilla, F., 2004. *Nature* 427 (6974), 548–553.
- Steel, B.C., McKenzie, D.R., Bilek, M.M.M., Nosworthy, N.J., dos Remedios, C.G., 2006. *Biophys. J.* 91 (6), L66.
- Steinhoff, H.J., Kramm, B., Hess, G., Owerdieck, C., Redhardt, A., 1993. *Biophys. J.* 65 (4), 1486–1495.
- Stuchly, M.A., Stuchly, S.S., 1980. *IEEE Trans. Instrum. Meas.* 29 (3), 176–183.
- Tanaka, M., Sackmann, E., 2005. *Nature* 437 (7059), 656–663.
- Terrettaz, S., Ulrich, W.P., Guerrini, R., Verdini, A., Vogel, H., 2001. *Angew. Chem. Int. Ed.* 40 (9), 1740–1743.
- Voets, T., Talavera, K., Owsianik, G., Nilius, B., 2005. *Nat. Chem. Biol.* 1 (2), 85–92.